Eur. Phys. J. D **5**, 237–242 (1999)

THE EUROPEAN PHYSICAL JOURNAL D

EDP Sciences

How to get access to long range states of highly excited molecules

M.-L. Almazor[1], O. Dulieu[1,a], M. Elbs[2], E. Tiemann[2], and F. Masnou-Seeuws[1]

[1] Laboratoire Aimé Cotton, Université Paris-Sud, Bâtiment 505, 91405 Orsay Cedex, France
[2] SFB 407, Institut für Quantenoptik, Universität Hannover, Welfengarten 1, 30167 Hannover, Germany

Received: 28 May 1998 / Revised: 5 August 1998 / Accepted: 24 September 1998

Abstract. Due to competition between ionic and covalent dissociation, the excited potential curves of the alkali dimers display long range structures, leading in some cases to secondary wells. We discuss the possibility of populating the well (with a depth of 1614.8 cm^{-1}, located at $R_e = 30.5a_0$) that is present in the Na_2 $(6)^1\Sigma_g^+$ potential curve and propose detection schemes.

PACS. 31.50.+w Excited states – 33.20.-t Molecular spectra – 33.70.Ca Oscillator and band strengths, lifetimes, transition moments, and Franck-Condon factor

1 Introduction

The existence of structures in the long range potential curves of the alkali dimer molecules offers opportunities to create long range molecules. Recent accurate *ab initio* calculations for Na_2 and K_2 [1,2] have demonstrated the presence of secondary wells, located at large internuclear distances, in the excited potential curves of $^1\Sigma_{g,u}^+$ and $^3\Pi_{g,u}$ symmetries. They correspond to avoided crossings due to a change of the electronic wavefunction from ionic to covalent character, and they lead usually to a rapid variation of the transition dipole moment matrix element. The possibility to populate long-range potential wells is of interest for schemes aiming at manipulating or cooling molecules [3,4].

The aim of the present work is to discuss the efficiency of an experimental scheme designed to transfer population from the ground state of Na_2 to some vibrational levels of a secondary well, and to propose a detection method. Recent calculations [1] predict a long range well in the $(6)^1\Sigma_g^+$ potential curve, located at $30.5a_0$ ($1a_0 = 0.0529$ nm) with a depth of 1614.8 cm^{-1}, which seems ideally suited for such purpose. Indeed, it is a gerade state correlated to the $Na(3s) + Na(5s)$ dissociation limit. A two-photon excitation scheme can be designed, with a first step populating a vibrational level in the $A^1\Sigma_u^+$ or in the $B^1\Pi_u$ potential curves, both correlated to the first excited asymptote $Na(3s) + Na(3p)$. The possibility to populate an arbitrary vibrational level of the $A^1\Sigma_u^+$ state has been demonstrated by recent experiments [5,6]. We shall therefore focus on the efficiency of the second step to transfer population to the secondary well in the $(6)^1\Sigma_g^+$ potential curve. A similar excitation scheme has been proposed by Tsai *et al.* [7] to populate levels of the outer well of the $(3)^1\Pi_g$ state in Na_2. In Section 2, we present the potential curves used in the present work. In Section 3, we report calculations of the excitation probabilities. In Section 4, we analyze the fluorescence decay to propose a detection scheme. In Section 5, we collect the results to demonstrate the feasibility of the experiment. Atomic units will be used except when otherwise stated.

[a] e-mail: dulieu@perceval.lac.u-psud.fr

2 Molecular potential curves and transition dipole moments

We have used in the present work the molecular potential curves computed by Magnier *et al.* [1] in the framework of *ab initio* calculations using effective potentials with accurate representation of core-polarization effects. The accuracy of the long range calculations have been shown to reach a few cm^{-1} [1,8,9]. The computed curves can be connected in the long range region ($R > 50a_0$) to asymptotic calculations [8]. The double well structure in the $(6)^1\Sigma_g^+$ potential curve, represented in Figure 1, consists of two minima located respectively 2810 cm^{-1} and 6643 cm^{-1} below the $(3s+5s)$ asymptote and an intermediate barrier, at distance $R = 15.15\,a_0$, located 1196 cm^{-1} below the asymptote. The inner well of this potential was studied by Tsai *et al.* [10], and is in good agreement with the *ab initio* result [1].

Several other potential curves of $^1\Sigma_g^+$ symmetry are also displayed in Figure 1. The (3) to (5) $^1\Sigma_g^+$ curves are correlated to the three $Na(3s) + Na(4s, 3d, 4p)$ dissociation limits located below the $Na(3s)+ Na(5s)$ asymptote. The $(7)^1\Sigma_g^+$ and $(8)^1\Sigma_g^+$ curves are dissociating into $Na(3p)+Na(3p)$. Avoided crossings, due to ionic-covalent

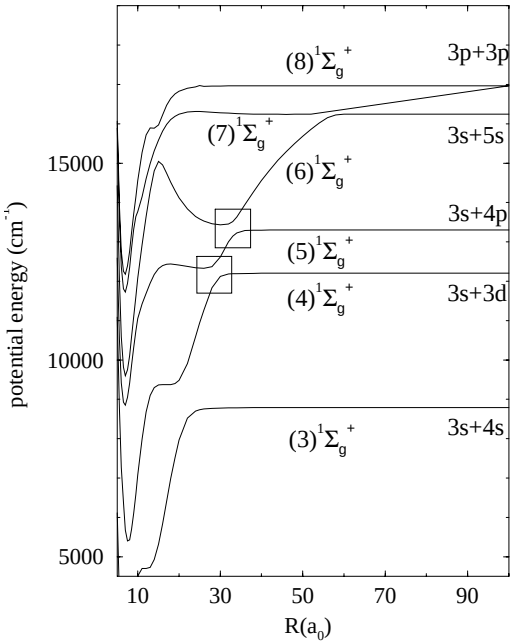

Fig. 1. Avoided crossings in the *ab initio* potential curves of symmetry $^1\Sigma_g^+$ in the range $5-100a_0$ of internuclear distances R. The track of an ionic diabatic curve correlated to the $Na^+ + Na^-(^1S_0)$ dissociation limit is clearly visible. The energy origin is chosen at the dissociation limit $Na(3s)+Na(3p)$.

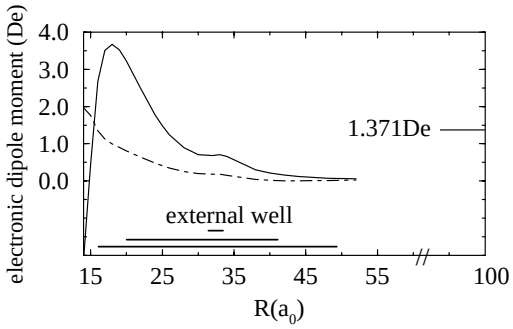

Fig. 2. Variation, as a function of the internuclear distance R, of the electronic dipole transition moment (in Debye) between the $(6)^1\Sigma_g^+$ state and the $A^1\Sigma_u^+$ state (solid curve) or the $B^1\Pi_u$ state (broken curve). The range of internuclear distances corresponding to the vibrational motion in the external well of the upper curve is indicated by bold lines for three values of the vibrational quantum number ($v_6 = 0$, $v_6 = 60$ and $v_6 = 118$). The minimum in the dipole moment corresponds to a distance where the upper state has ionic character. The calculations show that the atomic value for the dipole transition moment $5s-3p$ is indeed reached at $R = 100a_0$.

interaction, appear very clearly, in the region of the minimum of the secondary well in the $(6)^1\Sigma_g^+$ potential curve. We shall consider first a model neglecting predissociation and assuming that the adiabatic picture is valid. We shall discuss later on the limits of this model.

Both for the excitation and for the detection schemes, we should estimate the efficiency of radiative transitions towards the other electronic states, for which Franck-Condon principle gives a first indication. As the well in the $B^1\Pi_u$ curve is narrower than in the $A^1\Sigma_u^+$ curve, it is intuitively clear and will be demonstrated below that the Franck-Condon factors will be more favourable in the latter case. However, the transition probabilities are also governed by the electronic dipole moment matrix elements. The latter quantities were computed in the course of the *ab initio* calculations described in [1] in the 14–100 a_0 range of internuclear distances R. Data suitable for interpolation are available up to $52a_0$, and one calculation has been performed at $R = 100a_0$ to check the asymptotic behaviour. We display in Figure 2 the R variation of the two matrix elements defined using the conventions of [11] for the dipole moment:

$$|\boldsymbol{\mu}_{6A}(R)|^2 = |\mu^z_{6A}(R)|^2 = |\langle A^1\Sigma_u^+| \sum_{i=1,2} r_i \cos(\theta_i) |(6)^1\Sigma_g^+\rangle|^2 \quad (2.1)$$

and

$$|\boldsymbol{\mu}_{6B}(R)|^2 = |\mu^+_{6B}(R)|^2 = |\langle B^1\Pi_u| \sum_{i=1,2} r_i \sin(\theta_i)/\sqrt{2} |(6)^1\Sigma_g^+\rangle|^2 \quad (2.2)$$

In equations (2.1, 2.2), the summation is over the two active electrons involved in the molecular calculations. The ionic character of the long range potential curve of $(6)^1\Sigma_g^+$ in the $40a_0 < R < 60a_0$ region of internuclear distances is clearly manifested in Figure 2: starting in the asymptotic region from an allowed atomic transition $Na(5s) \rightarrow Na(3p)$ where the dipole moment is 1.371 De (1 Debye = 0.3935 a.u.), both curves go to 0 around $R = 52a_0$. At intermediate internuclear distances, in the region where avoided crossings are located, the dipole moment increases again to a value larger than the asymptotic one, due to the $3s+3d$ character of the molecular orbitals. We have indicated in the figure the typical range of the vibrational motion for various bound levels in the external well, suggesting that we may expect the main contribution to the transition probability at the *inner* Condon point and not at the *outer* one.

3 Calculation of excitation probabilities for $A^1\Sigma_u^+$-$(6)^1\Sigma_g^+$-transitions

In order to compute the energy and wavefunctions of the bound vibrational levels, we have used two different numerical methods: a Numerov-Cooley algorithm [12] and a Fourier Grid Hamiltonian method (FGH) [13,14]. For a correct description of the fast oscillations in the $\chi^A_{v_A}(R)$ vibrational wavefunctions of highly excited levels ($v_A > 80$) of the A state, we had to use a mesh of 100 points per a.u. for the Numerov method compared to 20 points per a.u. for the FGH method. The results obtained by both methods for the vibrational energies agree within $3\times10^{-3}\,\mathrm{cm}^{-1}$. We should recall that for sake of consistency we have used the computed potential curve for the A state and not an experimentally determined one. Indeed, the aim of this study is to estimate the experimental conditions about

Table 1. Computed vibrational energies G_{v_6} and rotational constants B_{v_6} of the outer well of the $(6)^1\Sigma_g^+$-state, with respect of the $3s+5s$ asymptote. We also give the level v_A of the $A^1\Sigma_u^+$-state with best Franck-Condon overlap, the corresponding Franck-Condon factors (FCF), and transition moments D_{v_6,v_A} as defined in equation (3.1).

v_6	G_{v_6} (cm^{-1})	B_{v_6} ($10^{-3}\,\mathrm{cm}^{-1}$)	v_A	FCF	$D^{6A}_{v_6,v_A}$ (De)
0	−2804.7	5.69	126	0.309	0.548
10	−2677.8	6.37	118	0.068	0.500
20	−2540.8	6.82	114	0.052	0.624
30	−2399.3	7.11	110	0.038	0.680
40	−2255.8	7.31	108	0.034	0.752
50	−2112.4	7.45	105	0.033	0.819
60	−1970.4	7.55	103	0.027	0.800
70	−1830.6	7.63	100	0.027	0.834
80	−1693.6	7.71	98	0.025	0.826
90	−1560.3	7.78	95	0.022	0.755
100	−1430.9	7.89	93	0.023	0.739
110	−1306.2	8.11	90	0.023	0.651

laser fields and detection schemes for sufficient sensitivity, thus internal consistency of potential energies and of internuclear dependence of transition moments is of concern. We do not claim that the latter given spectral energies can simply be used to look exactly only at this position to find the desired spectral feature.

The outer well of the $(6)^1\Sigma_g^+$ potential curve contains 118 vibrational levels with wavefunctions localized in the outer region, and two upper levels strongly coupled by tunneling with the levels in the inner well. We display in Table 1 the computed molecular constants for a sample of vibrational numbers v_6. In order to discuss a possible excitation scheme, we have computed the Franck-Condon factors $|\langle\chi^6_{v_6}|\chi^A_{v_A}\rangle|^2$, $|\langle\chi^6_{v_6}|\chi^B_{v_B}\rangle|^2$ and dipole transition moments

$$D^{6A}_{v_6,v_A} = |\langle\chi^6_{v_6}|\mu^z_{6A}(R)|\chi^A_{v_A}\rangle| \tag{3.1}$$

and

$$D^{6B}_{v_6,v_B} = |\langle\chi^6_{v_6}|\mu^+_{6B}(R)|\chi^B_{v_B}\rangle| \tag{3.2}$$

for the photo-excitation from bound vibrational levels in the $A^1\Sigma_u^+$ and $B^1\Pi_u$ potential curves. In the second case we found negligible values, due to the narrow shape of the B potential curve. From the wavefunctions drawn in Figure 3, we see that bound wavefunctions in the outer well of the $(6)^1\Sigma_g^+$ curve have non negligible overlap only with the continuum wavefunctions of the B curve, ruling out this excitation scheme. In contrast we find an efficient excitation scheme from the A state: all the long range v_6 vibrational bound levels can be reached from at least one bound level of the $A^1\Sigma_u^+$ state with a transition moment of at least 0.5 De. Typical values for the overlap integrals and transition dipole moments are given in Table 1.

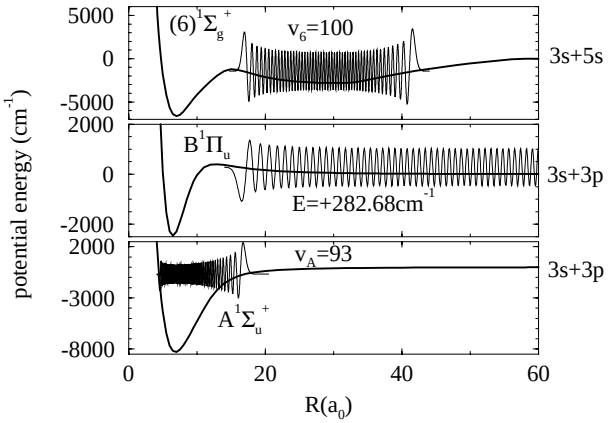

Fig. 3. Example of vibrational wave functions in the $A^1\Sigma_u^+$ curve (bottom) and in the outer well of the $(6)^1\Sigma_g^+$-state (top) with good Franck-Condon overlap. Also indicated is a typical continuum vibrational wavefunction for the $B^1\Pi_u$ curve. The energy origin is chosen at the dissociation limit Na($3s$)+Na($3p$) and Na($3s$)+Na($5s$), respectively.

The best Franck-Condon factors are for transitions where the inner turning point of the (6)-state level coincides with the outer turning points of A-state level, as is illustrated in Figure 3. This gives a narrow band of a few (3 to 4) A-state levels with Franck-Condon overlap larger than 0.01. In Section 5 we show that these transition moments are large enough for a spectroscopy experiment.

4 Decay processes

4.1 Spectral distribution of the fluorescence

In order to discuss the efficiency of the detection schemes, it is important to know the main channels of decay from the rovibrational levels (v_6, J_6) of the excited $(6)^1\Sigma_g^+$ electronic state. The general expression for the spontaneous emission probability to a rovibrational level $(v", J")$ of a lower electronic state f is:

$$A^{6f}_{v_6J_6,v"J"} = \frac{1}{4\pi\epsilon_0}\frac{64\pi^4}{3h}\nu^3_{v_6J_6,v"J"} \times\left\{\frac{1}{2J_6+1}\sum_{M_6}\sum_{M"}|\langle\Psi^6_{v_6,J_6,M_6}|\boldsymbol{\mu}(R)|\Psi^f_{v",J",M"}\rangle|^2\right\}. \tag{4.1}$$

In equation (4.1), $\nu_{v_6J_6,v"J"}$ is the frequency associated to the transition, and we have introduced the matrix elements of the dipole moment operator $\boldsymbol{\mu}$ defined in Section 2 using the conventions of [11] for unpolarized light. $\Psi^i_{v_6,J_6,M_6}$ and $\Psi^f_{v",J",M"}$ are the rovibrationnal wavefunctions associated to the magnetic sublevels in the initial and the final state. This general expression can be markedly simplified because, for the transitions that we consider, it is possible to neglect the variation, as a function of the rotational numbers J_6 and $J"$, of the transition

frequency and of the radial part of the rovibrational wavefunctions. Therefore, it is sufficient to perform the calculations assuming $J_6 = 0$, summing over the final J", and taking vibrational wavefunctions $\chi^6_{v_6}$ for the initial state and $\chi^A_{v_A}$ or $\chi^B_{v_B}$ for the final state. We define, for unpolarized fluorescence light, an effective spontaneous emission rate:

$$\overline{A^{6f}_{v_6,v"}} = \sum_{J"} A^{if}_{v_6 J_6, v" J'"} = \frac{1}{4\pi\epsilon_0}\frac{64\pi^4}{3h}\nu^3_{v_6 v"}(2-\delta_{\Lambda" 0})(D^{6f}_{v_6,v"})^2. \quad (4.2)$$

In equation (4.2), $D^{6f}_{v_6,v"}$ is equal to either $D^{6A}_{v_6,v_A}$ or $D^{6B}_{v_6,v_B}$ respectively defined in equations (3.1, 3.2). As in Section 3, the bound vibrational wavefunctions $\chi^6_{v_6}(R)$ and $\chi^f_{v"}(R)$ (with $f = A, B$) have been computed by the FGH method [14] and the integrals have been evaluated by standard trapezoidal quadrature. In order to compute the emission probability from the bound levels v_6 towards a vibrational continuum of the final electronic state the final radial wavefunctions for energy E" above the dissociation limit have been determined through a discretization procedure. The latter is automatically introduced owing to the finite size of the grid in the FGH treatment which generates unity-normalized pseudofunctions $\chi_{v"}(R)$, where the number v" is now labeling the discretized continuum states. We approximate the density of states by:

$$\rho_{E"} = \frac{\partial E}{\partial v}^{-1} \simeq \rho_{v"} = \frac{2}{E_{v"+1} - E_{v"-1}} \quad (4.3)$$

and energy-normalized functions through:

$$\chi_{E"}(R) = \sqrt{\rho_{E"}}\chi_{v"}(R). \quad (4.4)$$

As the transition probability is a slowly varying function of E", it is justified to introduce a probability density by:

$$\frac{dA^{6F}_{v_6,E"}}{dE"} = A^{6F}_{v_6,v"}\,\rho_{E"}. \quad (4.5)$$

The same procedure can be applied to bound levels by considering negative E" values and defining:

$$\frac{\Delta A^{6F}_{v_6,v"}}{\Delta E"(v")} = A^{6F}_{v_6,v"}\,\rho_{v"}. \quad (4.6)$$

For small values of v_6, there is negligible fluorescence to the continuum. For higher values of the initial vibrational level, the fluorescence process is populating both bound and continuum states. In Figure 4 we give as an example the probability of spontaneous emission of a photon from vibrational level $v_6 = 10$ to the bound and continuum levels of the $A^1\Sigma^+_u$ according to equations (4.5, 4.6). The continuity at threshold between discrete and continuum spectrum [15] is clearly manifested. We should note that due to neglect of fine structure, the threshold region is only approximately represented in our model. The probability densities for spontaneous emission to continuum levels of the $B^1\Pi_u$ state are roughly one order of magnitude smaller than for the A state.

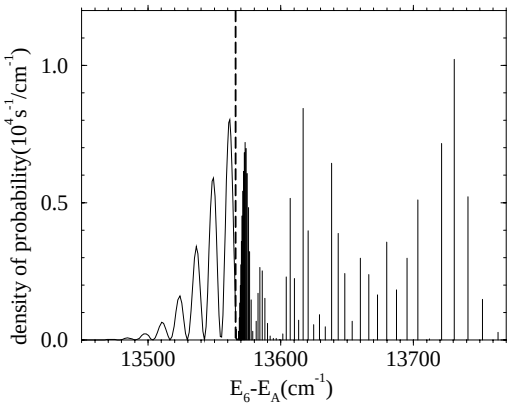

Fig. 4. Density of probability as defined in equations (4.5, 4.6) for spontaneous emission from the $v_6 = 10$ vibrational level of the upper well to various bound and continuum vibrational levels of the $A^1\Sigma^+_u$ state. The dashed line corresponds to the dissociation limit of the A state.

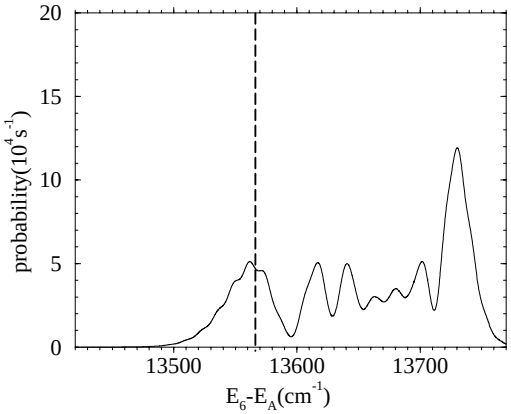

Fig. 5. Calculated fluorescence probability from the $v_6 = 10$ vibrational level of the upper well to various bound and continuum vibrational levels of the $A^1\Sigma^+_u$ state integrated on a 10 cm^{-1} Gaussian observation window.

Finally, in order to compare our calculations to experiment, we should take into account the width of an observation window. We reproduce in Figure 5 the result of a convolution between a Gaussian detection function with width of 10 cm^{-1} at half maximum, and truncated at 1% of maximum, with the computed probability densities for fluorescence towards A state starting from a $v_6 = 10$ level. A large contribution of the fluorescence decay will go to the continuum and is concentrated in a narrow spectral window. This will support an efficient detection scheme.

If we assume that the upper electronic state is dynamically uncoupled from the neighbouring states, and consider fluorescence towards the A and B lower states we obtain partial decay rates as:

$$\frac{1}{\tau^{if}_{v_6}} = \sum_{v"} A^{if}_{v_6,v"} \quad (4.7)$$

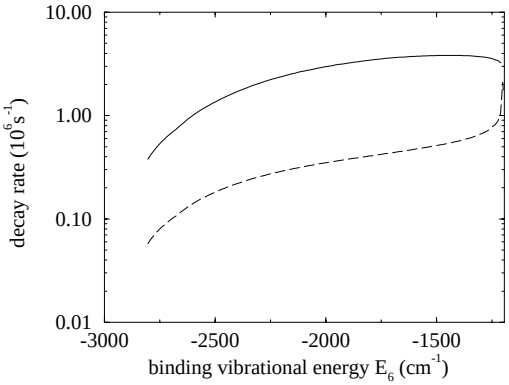

Fig. 6. Partial radiation decay rates (in $10^6\,\mathrm{s}^{-1}$), as defined in equation (4.7) in text, from vibrational level v_6 of the upper well to all bound and continuum vibrational levels of the $A^1\Sigma_u^+$ state (solid curve) and of the $B^1\Pi_u$ state (dashed curve). The binding energy is relative to the asymptote of the $(6)^1\Sigma_g^+$ curve.

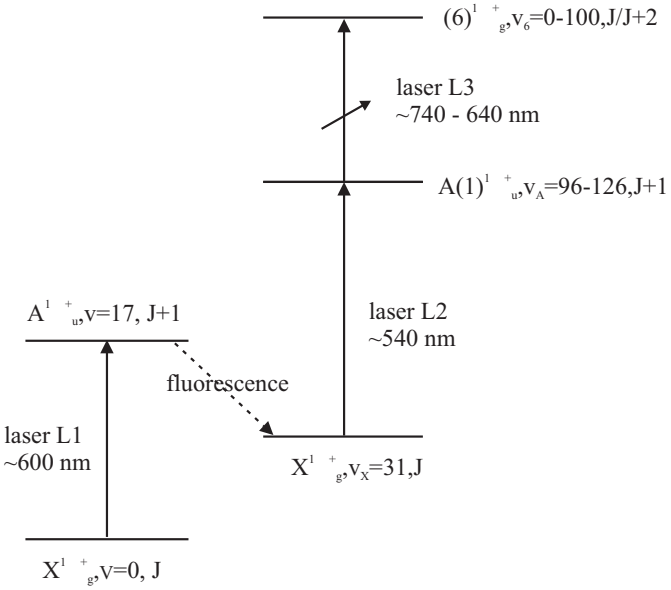

Fig. 7. Scheme of the experiment. Laser 1 (dye laser) populates rovibronic levels of $X^1\Sigma_g^+$ by Franck-Condon pumping. Lasers 2 and 3 (dye lasers) are arranged in STIRAP configuration to populate a chosen vibrational level of $(6)^1\Sigma_g^+$ and avoid population in $A^1\Sigma_u^+$.

where the summation over index v" includes the continuum.

The results are displayed in Figure 6, showing that the radiative decay to A state is one order of magnitude larger than to the B state, and increases by a factor of 5 moving from $v_6 = 0$ ($E_6 = -2800$ cm^{-1}) to the upper levels $v_6 \geq 100$ ($E_6 \geq -1430$ cm^{-1}). We could conclude that the radiation decay is very slow, so that the external well that we are considering is close to a metastable molecular state: however, the present model is not taking predissociation effects into account, and we shall discuss this point below.

Moreover, we have checked that when the excitation process through polarized laser light is populating selectively one magnetic sublevel, for instance $M_6 = 0$, equation (4.2) is also valid, so that the calculations above may apply to that case.

4.2 Predissociation effects

The potential curves $(5)^1\Sigma_g^+$ and $(6)^1\Sigma_g^+$ display an avoided crossing at about $R = 33.2a_0$ possibly leading to predissociation of all levels of the outer well in the state $(6)^1\Sigma_g^+$. Thus the partial radiative lifetimes of the order of 10^{-6} s (see Fig. 6) must be compared with the predissociation lifetimes and with radiative lifetimes associated to other decay processes. We have simply used the Landau-Zener model in order to estimate the transition probability to the lower curve correlated to the Na($3s$)+Na($4p$) dissociation limit, considering various vibrational levels. For a classical vibrational motion corresponding to zero value of the impact parameter, the typical transition probability P_1 for a single passage varies between 5×10^{-10} for $v_6 = 0$ and to 1.6×10^{-3} for $v_6 = 100$. To estimate the order of magnitude we simply sum up the passages incoherently: this assumption may be reasonable, because the wave-packets moving in $(5)^1\Sigma_g^+$ potential split further at additional crossing points. As we neglect any flux coming back from the decay channels, such estimation gives us an upper limit of the loss probability, from which we deduce a lower limit τ_p for the predissociation lifetime. Considering that the time delay between two successive passages is half the vibration period, we can compute the evolution of the population of a v_6 level and hence the predissociation lifetime τ_p. For low v_6 values ($0 \leq v_6 \leq 10$), the resulting predissociation lifetime is $\tau_p \geq 2 \times 10^4$ ns, *i.e.* one order of magnitude larger than the radiative lifetimes $\tau_r \geq 1400$ ns found in Section 4.1. Then, the $(6)^1\Sigma_g^+$ vibration channels can safely be considered as dynamically isolated from the neighbouring ones in the region of large internuclear distances ($10 < R < 40a_0$), and the fluorescence is indeed the dominant decay process. In contrast, for $v_6 = 20$, the predissociation lifetime reaches values $\tau_p = 600$ ns comparable to the radiative lifetime $\tau_r = 820$ ns. For the upper levels, we find even smaller values: the predissociation lifetime for $v_6 = 100$ is found around 0.8 ns, while $\tau_r = 260$ ns, two orders of magnitude larger. Therefore the levels are still narrow, but a detection scheme involving cascade process from the atomic $4p$ level to $3d$ and $3s$ should be considered.

5 Experimental scheme

With these results, we are now able to discuss the feasibility of a spectroscopic experiment. Because direct transitions from $X^1\Sigma_g^+$ to $(6)^1\Sigma_g^+$ are dipole-forbidden we have to use a two-photon scheme, to populate $(6)^1\Sigma_g^+$, using rovibronic levels of the $A^1\Sigma_u^+$ state as intermediate levels. Due to favorable Franck-Condon factors, the vibrational

levels in the range of $v_A = 90$ to 126 are best suited for this purpose (see Tab. 1). These levels can be reached *via e.g.* $X^1\Sigma_g^+$, $v_X = 31$ which can be populated by Franck-Condon pumping from $v_X = 0$ *via* $A^1\Sigma_u^+$, $v_A = 17$ in a molecular beam [5]. A possible experimental scheme, using three lasers, is shown in Figure 7. By lasers 1 and 2 we specify a chosen J, leading to simplified spectra, when scanning laser 3.

The radiative lifetimes of the levels of the outer well of $(6)^1\Sigma_g^+$ ($\tau_r = 0.25\,\mu$s to 2.5 μs, see Fig. 6) are by far longer than those of the intermediate levels of $A^1\Sigma_u^+$ (about 12 ns [16]). Therefore, we have to use a coherent excitation scheme in order to avoid population of the intermediate level. It has been shown, that the STIRAP (Stimulated Raman Scattering with adiabatic passage) configuration with two near-resonant overlapping laser fields arranged in the counterintuitive order in space or time is able to transfer nearly 100% of the population from one ground state vibrational level towards another one, using levels of the $A^1\Sigma_u^+$ state as intermediate levels [17]. To estimate the efficiency of this configuration in our case, we have to compare the accessible Rabi frequencies. Assuming a laser intensity of 1000 W/cm^2, which can be achieved with a power of 100 mW focussed down to 100 μm^2 and a transition dipole moment $D^{6A} > 0.1$ De for the transition $A^1\Sigma_u^+$ to $(6)^1\Sigma_g^+$, we get Rabi frequencies of $\Omega_R > 300$ MHz. For the transitions from $X^1\Sigma_g^+$ $v_X = 31$ to $A^1\Sigma_u^+$, $v_A = 90$ to 126 we calculate transition dipole moment of at least $D^{AX} = 0.1$ De leading to Rabi frequencies in the same range. With these Rabi frequencies we calculate a population transfer of more than 90% for the STIRAP configuration. Even a reduction of the laser intensities by a factor of 15 will allow to transfer more than 50% of the population.

For the detection we have to distinguish different cases depending on the predissociation rates. For levels with negligible predissociation we will observe the fluorescence $A^1\Sigma_u^+$–$(6)^1\Sigma_g^+$. As shown in Figure 4 a large part of the fluorescence will be shifted to the red (13 550 cm^{-1}) compared to the exciting laser frequency (13 700 cm^{-1}). Therefore, it will be possible to introduce a spectral filter in order to separate this part of the fluorescence from scattered laser photons. Moreover, this filter will suppress the fluorescence from intermediate levels v_A. By this way it will be possible to observe the fluorescence with low background.

When the predissociation rate becomes of the order of the radiative rate, it will be preferable to observe the dissociation by the atomic fluorescence on the transition $4p$–$3s$: this scheme will improve signal-to-noise ratio because of spectral narrowing of the fluorescence and easy background suppression. The predissociation will lead to slightly broadened lines, as discussed in Section 4. However, we expect little influence on the STIRAP process as long as the resulting levels remain narrower than the experimental resolution, which we estimate to be around 10 MHz, due to saturation and time of flight broadening, residual Doppler and laser width.

6 Conclusion

We have discussed the feasibility of an experimental scheme designed to transfer population to a long range well of a highly excited Na_2 molecule. In such a well, the vibrational motion is confined to the $15a_0$–$50a_0$ range of internuclear distances. Using accurate data for the potential curves and dipole transition moments, we have computed the transition probabilities for a two-step excitation scheme. From those results and discussion of a STIRAP experiment, we may conclude that it will be possible to transfer at least 50% of the population in $X^1\Sigma_g^+$ $v_X = 31$ to a given vibrational level of $(6)^1\Sigma_g^+$. The fluorescence from these levels will be observable with low background, leading to sufficient signal-to-noise in the detection. Due to the large value of the lifetime, such levels can be considered as metastable levels which are interesting for manipulating molecules.

The authors are grateful to Drs Sylvie Magnier and Philippe Millié for providing transition dipole moment data. This work has benefited of the PROCOPE program between France and Germany.

References

1. S. Magnier, Ph. Millié, O. Dulieu, F. Masnou-Seeuws, J. Chem. Phys. **98**, 7113 (1993).
2. S. Magnier, Ph. Millié, Phys. Rev. A **54**, 204 (1996).
3. J.T. Bahns, P.L. Gould, W.C. Stwalley, J. Chem. Phys. **104**, 9689 (1996).
4. A. Fioretti, D. Comparat, A. Crubellier, O. Dulieu, F. Masnou-Seeuws, P. Pillet, Phys. Rev. Lett. **80**, 4402 (1998).
5. E. Tiemann, H. Knöckel, H. Richling, Z. Phys. D **37**, 323 (1996).
6. M. Elbs, O. Keck, H. Knöckel, E. Tiemann, Z. Phys. D **42**, 49 (1997).
7. C.-C. Tsai, J.T. Bahns, W.C. Stwalley, J. Chem. Phys. **99**, 7417 (1993).
8. S. Magnier, M. Aubert-Frécon, O. Bouty, F. Masnou-Seeuws, Ph. Millié, V.N. Ostrovskii, J. Phys. B **27**, 1723 (1994).
9. C.-C. Tsai, J.T. Bahns, H. Wang, T.-J. Whang, W.C. Stwalley, J. Chem. Phys. **101**, 25 (1994).
10. C.-C. Tsai, J.T. Bahns, W.C. Stwalley, J. Mol. Spectrosc. **167**, 429 (1994).
11. E.E. Whiting, A. Schadee, J.B. Tatum, J.T. Hougen, R.W. Nichols, J. Mol. Spectrosc. **80**, 249 (1980).
12. J.M. Blatt, J. Comp. Phys. **1**, 382 (1967).
13. R. Kosloff, J. Phys. Chem. **92**, 2087 (1988).
14. O. Dulieu, P.S. Julienne, J. Chem. Phys. **103**, 60 (1995).
15. A.C. Allison, A. Dalgarno, J. Chem. Phys. **55**, 4342 (1971).
16. G. Baumgartner, H. Kornmeier, W. Preuss, Chem. Phys. Lett. **107**, 13 (1984).
17. U. Gaubatz, P. Rudecki, S. Schiemann, K. Bergmann, J. Chem. Phys. **92**, 5363 (1990).